Protein Separation by Continuous-Flow Electrophoresis in Microgravity

Michael J. Clifton, Hélène Roux-de Balmann, and Victor Sanchez
Laboratoire de Génie Chimique (CNRS URA 192), Université Paul Sabatier, 31062 Toulouse cedex, France

During the IML-2 space shuttle mission, the RAMSES instrument was operated in the Spacelab module. This continuous-flow electrophoresis device performs separation and purification of protein solutions on a preparative scale. Samples containing artificial mixtures of pure proteins were used to test the capabilities of the device, and useful separations were obtained for proteins having a mobility difference of only 3×10^{-9} $m^2 \cdot V^{-1} \cdot s^{-1}$. *Operating conditions that cannot be applied on earth were explored for two different sample concentrations, one of which is too high to allow treatment on earth. It agrees well with a previously published numerical model in that the main cause of loss in resolution in this process is the electrohydrodynamic spreading of the protein filaments.*

Introduction

Electrophoresis is the basis for the most powerful techniques now used in analyzing mixtures of biological macromolecules. Various processes also exist that allow these separations to be scaled up to a preparative level. Among these, continuous-flow zone electrophoresis (CFE) has the advantage of allowing a continuous operation and can be applied to a very wide range of biological material, including particulate matter, such as cells and cell fragments. When applied to proteins, it allows them to be separated at rates of around 100 mg/h while keeping them dissolved in an aqueous medium with little contact with solid surfaces, thus reducing denaturation. This process was introduced in the 1950s (Hannig, 1967), and some equipment is commercially available, but its application to protein separation has been hampered by the complexity of the system and by the lack of knowledge concerning the basic transport phenomena involved.

In this process, a carrier buffer solution is made to flow through a thin rectangular chamber. Electrode compartments on either side of the chamber are used to apply an electric field across its width. The solution containing the protein mixture to be separated is injected into the flowing buffer at the chamber inlet, in the form of a fine liquid filament. The proteins are carried along the length of the chamber and at the same time migrate under the influence of the electric field. At the pH fixed by the buffer, each protein species has a characteristic mobility, so the initial single filament separates into a series of filaments, one for each protein species. The different protein streams can be collected as separate fractions at the chamber outlet (Figure 1). The lateral distance through which each protein migrates is given by the product of its mobility with the field strength and the residence time spent in the electric field.

One of the major difficulties with CFE has been the presence of natural convection. This arises from density differences both within the carrier buffer and between the injected sample and the carrier buffer. The difference in composition between the injected sample and the carrier buffer (a very dilute solution) is accompanied by a difference in density that can cause the sample to fall through the carrier medium. Thus the residence time spent in the field is modified by the natural convection, and sample concentrations have to be limited to low values to keep the filament stable. Within the carrier buffer itself, the ion concentration is modified near the electrode compartments: this is in itself a source of density differences (Heinrich and Wagner, 1992; Heinrich et al., 1993). However, the passage of electric current through the conducting medium of the buffer causes heating by the Joule effect. The overall effect of Joule heating can be compensated by satisfactory cooling, but a greater problem is created by the nonuniformities in ion concentration causing a nonuniform heating that tends to amplify the density differences due to differences in concentration (Jouve and Clifton, 1991).

A possible solution to the problem of natural convection is to operate in a low-gravity environment, that is, inside orbiting space craft. Various attempts at performing electrophoresis experiments in space have been made in the past by

Correspondence concerning this article should be addressed to M. J. Clifton.

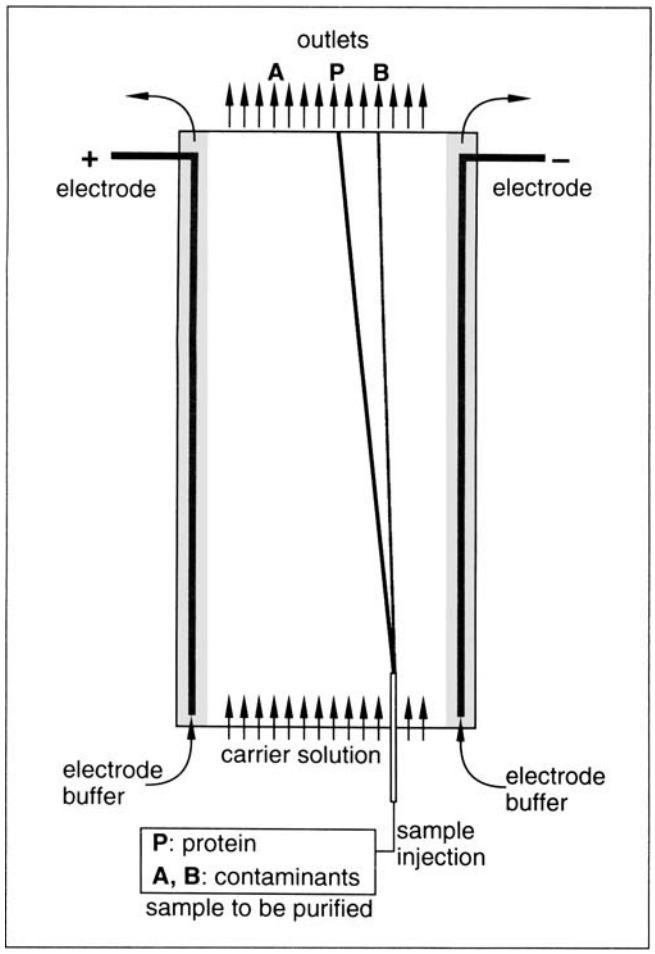

Figure 1. Principle of continuous-flow zone electrophoresis.

American, Russian, German, and Japanese teams. However, probably the most ambitious project was the one set up by the McDonnell Douglas Astronautics Company, which had its own astronaut operating a very large piece of equipment on quite a number of shuttle flights in the period 1982–1985. Some interesting results were obtained, but very few of the data were ever published. During two flights, the hardware was made available to NASA researchers who found that the sample filaments underwent considerable spreading unless the sample conductivity was made equal to that of the carrier buffer (Snyder et al., 1987). This phenomenon was later explained in terms of electrohydrodynamics (Rhodes and Snyder, 1987; Rhodes et al., 1989): the difference in conductivity between the filament and the carrier distorts the electric field, thus creating stress in the liquid that causes the local flow pattern that is responsible for the spreading. If the filament is of higher conductivity than the surrounding medium, then it is spread in the direction of the field; a filament of lower conductivity is spread in the direction perpendicular to the field. As protein molecules almost always increase the conductivity of solutions in comparison with the original buffer, the filaments are usually spread in the direction of the field, thus reducing the resolution of the process. This phenomenon is independent of gravity, and as it is not related to migration but rather to the dielectric response of the water dipoles, it occurs with both DC and AC fields (Rhodes et al., 1989; Clifton et al., 1992).

Other mechanisms for the distortion of protein filaments can appear in combination with the electrohydrodynamic effect. First, the carrier flow in the chamber has a parabolic profile. So the residence time of the protein in the chamber is not uniform across the chamber thickness: it is longer near the wall and shortest in the central plane. Second, the walls of the chamber carry fixed charges that, under the influence of the applied electric field, create an electroosmotic slip velocity at the wall. As the edges of the chamber are closed off, the overall effect is to introduce flow in the field direction with a parabolic velocity profile. Both these effects distort the initially circular cross section of the injected filament into a crescent shape (Strickler and Sacks, 1973). To reduce these effects, the injected filament diameter has to be less than about 30% of the chamber thickness. In the RAMSES experiments, this ratio was close to 20%

The RAMSES device is a continuous-flow electrophoresis instrument that was flown on the IML-2 shuttle flight in July 1994. A series of experiments was performed to observe protein separations under a variety of conditions, many of which are not possible on earth. The present authors performed three experiments in which the samples treated contained artificial mixtures of pure proteins. These samples are thus sufficiently well defined to allow comparison of the experimental results with a numerical model. The RAMSES device has a 40-channel on-line UV photometer that allows protein concentrations in the separated fractions to be monitored. For each experiment, one set of samples of these fractions could be collected.

The first experiment involved a sample containing two colored proteins very different in mobility (and thus easy to separate); the operating conditions used are applicable on earth. This experiment was intended to test the initial performance of the system. In the samples collected, both proteins were recovered pure.

In the second experiment, two colorless proteins with a small difference in mobility (3×10^{-9} $m^2\cdot V^{-1}\cdot s^{-1}$) were observed using different combinations of field strength and residence time. Among these, the observations at long residence times are not reproducible on earth, as a slow forced flow is particularly sensitive to disturbances by natural convection. However, this second sample was still sufficiently dilute to allow it to be treated on earth. The separated fractions were collected using the last set of conditions: about 80% of each protein was recovered pure.

For the third experiment, the same proteins were used as for the second, but at a concentration ten times higher (too concentrated to be used on earth), and once again different combinations of field strength and residence time were applied. Observations were made and for the final set of conditions, samples were collected. In this case, 26% of one protein was recovered pure, while the second protein remained contaminated.

A previously developed numerical model (Clifton, 1993) was applied to this system in a slightly simplified form. The good agreement between the model and the experimental results confirms the hypothesis that filament spreading is mainly caused by electrohydrodynamics. This means that a basis now exists for future optimization of this process.

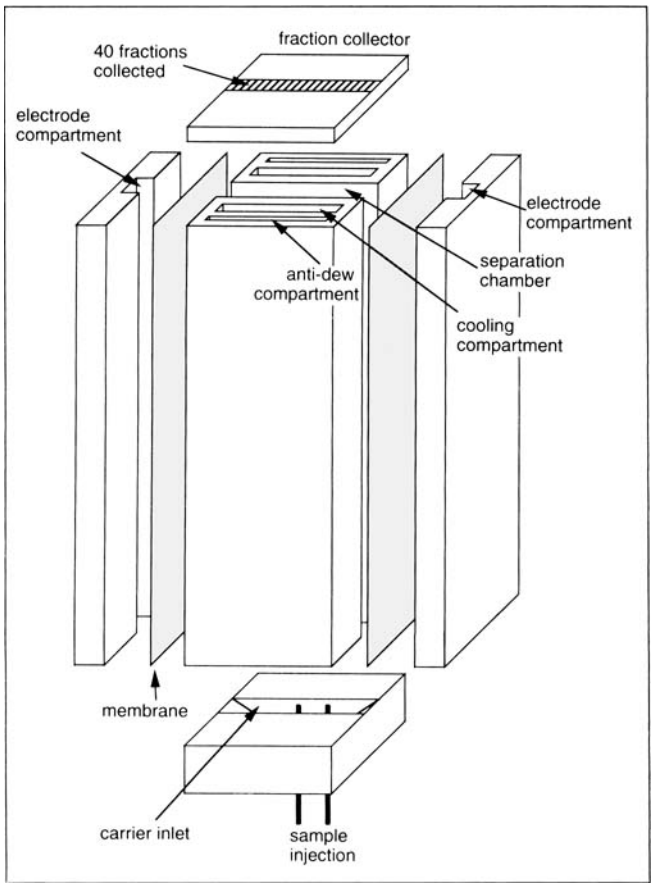

Figure 2. Exploded view of the RAMSES separation chamber.

The drawing is not to scale.

Experimental Equipment

The RAMSES device for CFE in microgravity was built by a consortium of French, Belgian, and Spanish companies. It occupied a single rack in the Spacelab module on board the shuttle *Columbia* and was flown on the IML-2 (Second International Microgravity Laboratory) mission in July 1994. Its presence on this 14-day flight was sponsored by the CNES, the French Space Agency.

The RAMSES separation chamber (Figure 2) has the following internal dimensions: 300 mm long, 41 mm wide, and 3 mm thick. Its polycarbonate walls are 4 mm thick. Cooling compartments are situated on the front and back walls that allow them to be cooled by a fast-flowing cooling liquid. Outside the cooling compartments, there are antidew compartments containing dry air, to prevent water vapor from condensing on the chamber. All the walls of these compartments are of polycarbonate polished to an optical-quality surface finish to achieve a high transparency.

The electrode compartments on either side of the chamber allow a field to be applied along the whole chamber length. They are separated from the chamber by ion-exchange membranes positioned so that the concentration polarization gives an enrichment of ions within the chamber and a depletion in the electrode buffer. This buffer is circulated through the compartments at a relatively high velocity so as to improve mass transfer at the membrane surfaces and to prevent gas bubbles from stagnating at the electrodes. The electrodes are gold wires at which gaseous hydrogen and oxygen are given off.

At the chamber inlet, the carrier buffer enters through a conical connector that allows a smooth passage from the circular inlet tube to the rectangular chamber slit. Within this inlet zone, two sample injectors are located: one at the middle of the chamber width, the other near the side. Hollow glass needles are used to inject the sample solution into the carrier flow. These needles have to be very precisely centered in the chamber thickness. This centering was performed during ground operations about 10 months prior to the flight, but the experimental results show that a good centering was maintained.

At the chamber outlet, the carrier solution leaves the chamber through a fraction collector: this has a series of funnel-shaped outlet ports that allow the liquid to be separated into 40 different streams (one per millimeter) without disturbing its flow.

Four independent fluid circuits are associated with the separation chamber. These are represented in Figure 3. The temperatures of the three major circuits can be controlled independently by the Fluid Cooling Module (FCM), made up of air-cooled Peltier elements. The first circuit contains the carrier buffer. This buffer, used for all experiments, was a "tris-borate" solution with a pH of 8.1 and an electrical conductivity of 140 μS/cm. The buffer is held in an 11-L tank, from which it flows through the FCM to the separation chamber. On leaving the chamber, the 40 separate streams pass through the on-line UV photometer, then through the carrier pump (a 40-channel peristaltic pump), before reaching the fraction collector. This device has two positions: in the "waste" position all 40 streams are directed together into a waste tank and in the "collect" position the 40 streams are collected in 40 sterile glass vials.

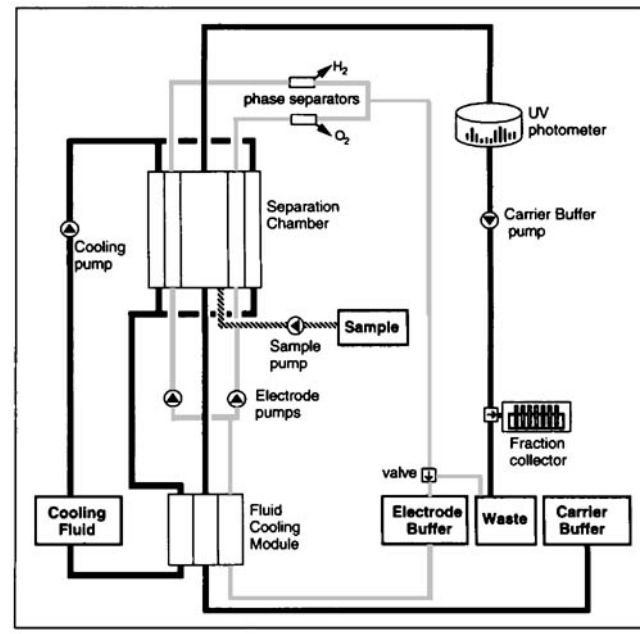

Figure 3. Hydraulic circuits of the RAMSES facility.

The second circuit is the electrode buffer circuit: during experimental operations, this is a closed loop. This buffer leaves its tank and passes through the FCM to fix its temperature at the required value. Two independent gear pumps are used for feeding the anode and cathode compartments. From each electrode compartment, the buffer goes through a phase separator to remove gas bubbles: these hollow-fiber membrane devices are commercially available artificial lungs, normally used for blood oxygenation. The buffer then returns to its tank. Provision is made for the electrode buffer to be diverted to a waste tank: this is used during an initial rinsing step.

The cooling fluid (sterile distilled water) is pumped around a closed loop: situated on this loop are an insulated tank, the cooling compartments of the separation chamber, a gear pump, and the FCM. The final circuit is the sample circuit; this is the only one without temperature control. The sample cassette consists of a polyvinyl chloride (PVC) bag containing the sample, a length of tubing that goes around the head of the peristaltic sample pump, and a septum. When the cassette is pushed into place, the septum is pierced by a thoroughly protected hypodermic needle. The sample can then flow through the needle into the line that leads to the injection port. Two different cassette positions are available corresponding to the two different injection points.

The tanks holding the three liquids are collapsible plastic bags held in a metal box. As the various buffer fluids had to be mounted into the system about six months before launch, a particular plastic material was used that is highly impermeable to air. In this way the solutions, particularly the carrier buffer, were able to be kept degassed up till the time of flight. The sample cassettes were able to be installed during "late access," about 24 hours before launch.

The on-line UV photometer allows the 40 carrier fractions to be monitored continuously for protein content by measuring their optical density at a wavelength of 278 nm. The 40 streams flow through quartz cuvettes that are arranged in a circle. A sensor arm rotates from one cuvette to the next and makes a complete set of measurements every 4 min: each measurement includes correction by a comparison with a blank cuvette, then with a closed shutter, to compensate for drift in the detector. During the flight, the results of these measurements were available to the crew member performing the experiment, and were included in the data sent down to the control center on the ground.

An alternative design for a UV detector is to have quartz windows set into the walls of the chamber and to use a UV source with a diode array to scan the solution. This design was not adopted for RAMSES for several reasons: quartz is considered a hazardous material for manned spaceflight, so the level of containment required for this design means that the chamber would have been hidden from view; moreover this system does not give the optical density in the fractions actually collected; and finally the use of a diode array implies a higher level of noise in the signal, as continuous correction with a blank cuvette is no longer possible. This type of design was used, however, for the Japanese FFEU electrophoresis device that also flew on IML-2.

Various pressure and temperature sensors are located at strategic points in the system. In particular, one temperature sensor is located at the chamber inlet and three more at different positions across the chamber outlet.

Experimental Procedures

For experiments to be performed by astronauts during a space flight, the procedures to be followed have to be defined in great detail many months in advance. During the flight, only minor modifications to the procedures can be made. The three experiments presented here followed two different plans: the first experiment was a relatively simple "direct separation," while the other two were more complex "optimization" experiments. The operating conditions for the different experiments are given in Table 1. The field strength E_0 given here is calculated from the current density and the electrical conductivity of the carrier solution at the measured temperature of the chamber.

In all experiments, the proteins used were commercial laboratory-grade products, purchased in a lyophilized form from the Sigma Chemical Company, St. Louis, MO. The buffer was prepared by Soludia S.A., Fourquevaux, France, from analytical-grade orthoboric acid and tris(hydroxymethyl)-aminomethane, $(HOCH_2)_3CNH_2$ (commonly called "tris" or THAM) to have a pH of 8.1 and a conductivity of 140 μS/cm for the carrier buffer and 250 μS/cm for the electrode buffer. The solution was then sterilized by ultrafiltration and degassed before being loaded into the buffer tank. All sample cassettes were prepared under sterile conditions. After dissolution of the lyophilized protein in the carrier buffer, the 30 mL of solution was dialyzed against 1.5 L of buffer for 24 h.

Table 1. Operating Conditions Used During the Experiments*

Exp.	Phase	$\Delta\Phi$ V	E_0 V/m	Q mL/h	U_0 mm/s	Q_s mL/h	T °C
E1	Collection	100	1,800	400	0.9	1.6	20.0
E2	A	120	2,100	310	0.7	1.15	20.0
	B	120	2,000	490	1.1	1.8	20.0
	C	160	2,700	490	1.1	1.8	20.0
	D	160	2,800	310	0.7	1.15	23.0
E3	A	80	1,500	310	0.7	1.15	21.5
	B	80	1,500	490	1.1	1.15	21.5
	C	160	2,700	490	1.1	1.15	22.5
	D	120	2,200	310	0.7	1.0	21.8

*Fractions were collected in phases E2D and E3D. $\Delta\Phi$ = applied voltage; E_0 = field strength; Q = carrier buffer flow rate; U_0 = mean carrier buffer velocity; Q_s = sample injection rate; T = chamber temperature.

The samples were then degassed and injected through an ultrafilter into the sterile sample cassette.

The sample used in the first experiment (E1) was a mixture of bovine serum albumin (BSA, colored with bromophenol blue) and bovine hemoglobin; both proteins were at a concentration of 3.0 g/L. Colored proteins were used here so that for this first use of the equipment the operator would have no difficulty in observing the trajectory of the proteins during separation. As it happened, this was a good choice, as it was found at the beginning of this experiment that the chamber contained a large bubble (about 2 cm in diameter) on one side, near the inlet to the chamber. When the sample was injected, it was seen to flow around the bubble, and the filament was only displaced and not disturbed by the presence of the bubble. Happily the carrier buffer had remained degassed and the bubble gradually dissolved during the operations. By the beginning of the fifth experiment (performed by another team, so not described here), it had completely disappeared.

In experiment E1, the sample was first injected without any field being applied. Its initial position at the outlet was observed using the readings of the UV photometer. Because of the bubble, the filament injected at the center of the chamber in this experiment was displaced from the fraction 20 to fraction 15. Then the temperature of the cooling liquid was adjusted and the field was applied. The migration of the proteins was followed by means of the UV photometer and when the position of the peak showing the presence of the protein had been stabilized, the sample collector was put into the collection position. Solution was collected for 28 min; at the carrier flow rate used this means a volume of about 4.7 mL in each sample tube. Then the collector was put back into the "waste" position and the voltage was cut. The six fractions thought to contain most protein were stowed in a refrigerator at 5°C and the other samples were stored at room temperature.

The sample for the second experiment (E2) was a mixture of BSA (2.8 g/L) and α-lactalbumin (2.2 g/L). This is a relatively dilute solution, but the proteins here have very similar electrophoretic mobilities and so are much more difficult to separate. The procedure for this "optimization" experiment was more complicated than for the previous one. Once the zero-field trajectory had been observed, a series of observations were performed using the UV photometer with different combinations of applied voltage and carrier flow rate and in the last phase, a fraction collection was performed.

During the observation phase, the temperature of the cooling liquid was adjusted each time the field strength was changed. The heat-transfer properties of the chamber and the liquid circuits had been calculated on the basis of tests performed on the ground and this allowed a suitable cooling temperature to be calculated so that the temperature variations within the chamber were minimized (Clifton and Marsal, 1989).

For the collection phase, the conditions used were those applied during the fourth part of the observation phase (highest field strength and longest residence time). The fractions were collected for 18 minutes; this corresponds to a volume of about 2.3 mL collected. Here the eight fractions containing protein were stowed in the refrigerator and the others were kept at room temperature.

For the third experiment (E3), the sample contained the same proteins as for E2, but at much higher concentrations: BSA at 26 g/L and α-lactalbumin at 21.6 g/L. Such concentrated samples cannot be treated on the ground because they have too high a density compared with the carrier buffer. Here the same procedure was followed as in experiment E2, except that different values of field strength and carrier flow rate were used. The separated fractions were collected for 15 minutes; this corresponds to a volume of 1.9 mL collected for each fraction. Eight fractions were kept refrigerated.

It should be noted that because of weight and space restrictions, only one sample-collection tray was available for each experiment: so only one set of fractions could be collected for each experiment. The same restrictions explain why only a small number of vials could be stored refrigerated. These restrictions are part of the price paid for operating in microgravity. Other restrictions are also worth mentioning: the experimental details have to be fixed many months, or even years, in advance and then when the experiments are performed difficulties inevitably arise. The astronauts are on a very tight schedule, so any delays mean loss of data. Last minute changes to experimental conditions are imposed by circumstances and experiments have to be shortened: this was the case for both experiments E2 and E3. So the use of the word "optimization" to describe these two experimental plans gives an idealized view of the conditions under which they were implemented.

After the flight, the collected fractions were recovered during the "early access" period, within 24 hours of the landing time. All collection tubes were rapidly deep-frozen before being sent back to France, where they were analyzed within a period of three weeks after reception.

Results and Discussion

Figure 4 shows the distribution of protein in the fractions collected during experiment E1. It can be seen that the two proteins, BSA, and hemoglobin were completely separated.

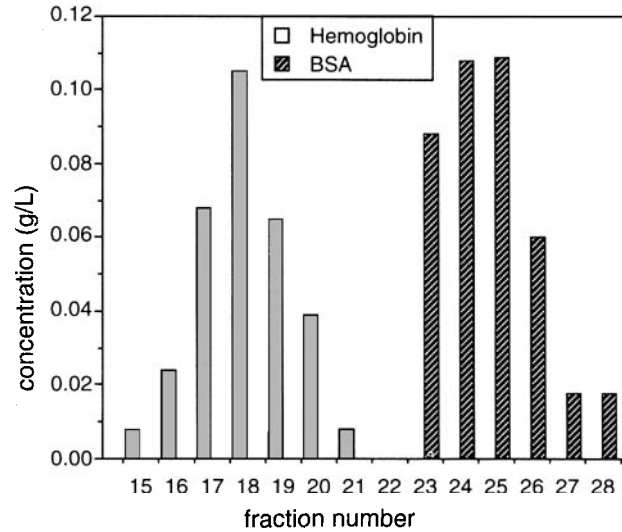

Figure 4. Protein concentrations in the different fractions collected during experiment E1.

Here the anode is on the right. Under zero-field conditions, the protein was located in fraction 15.

Table 2. Properties of Protein Solutions Used in Numerical Modeling

Exp.	Protein	Mobility $m^2 \cdot V^{-1} \cdot s^{-1}$	c_i^o g/L	$10^{11}\, D_i$ m^2/s	$10^3\,[\eta]$ L/g	d_i L/g	$\lambda_i c_i^o$ $\mu S/cm$
E2	BSA	-21.7×10^{-9}	2.8	6.0	3.7	0.17	7.1
	α-lactalbumin	-18.5×10^{-9}	2.2	10.6	3.01	0.17	15.4
E3	BSA	-21.7×10^{-9}	26	6.0	3.7	0.17	66
	α-lactalbumin	-18.5×10^{-9}	21.6	10.6	3.01	0.17	151

When compared with tests performed on the ground, it is found that each protein migrated the same distance from the zero-field position as in the ground tests. This means that the only effect of the presence of the bubble was to displace the protein filament: it had no effect on the degree of separation obtained for the two proteins.

The results of experiments E2 and E3 were compared with the predictions of a previously published numerical model (Clifton, 1993). A summary of the basis for this model is given in the Appendix. It takes into account the various phenomena that are known to cause the protein filament to change shape during its passage through the chamber: nonuniform residence times due to Poiseuille flow, electroosmosis, electrophoretic migration in a nonuniform field, variations in pH and conductivity due to differences in mobility of the various ionic species (electrokinetic or Kohlrausch effects), and electrohydrodynamics. To apply this model in the present case, it was slightly simplified: each protein was assumed to migrate with a constant mobility and the overall electrical conductivity at each point was calculated on the basis of the following formula:

$$\kappa = \kappa_0 + \lambda_1 c_1 + \lambda_2 c_2, \tag{1}$$

where κ_0 is the conductivity of the buffer without protein, and c_1 and c_2 are the concentrations of the two proteins. The λ coefficients were empirical constants determined by diafiltration of a 30 g/L solution of each protein using the same buffer as for the RAMSES experiments. The diafiltration was continued until a constant λ value was reached.

Table 2 shows the properties of the protein solutions that were assumed for the numerical calculations. The protein mobilities were measured by capillary electrophoresis in the same buffer. The $\lambda_i c_i$ values are for each protein at the initial sample concentration. The solution viscosity η was taken to be dependent on protein concentration in the following way:

$$\eta = \eta_w(1 + [\eta]_1 c_1 + [\eta]_2 c_2), \tag{2}$$

where η_w is the viscosity of water; the values of the intrinsic viscosities $[\eta]_i$ and the diffusion coefficients D_i are values compiled by Tyn and Gusek (1990). The dielectric permittivity ϵ of the solution was assumed to be dependent on protein concentration in the following manner:

$$\epsilon = \epsilon_0(D_w + d_1 c_1 + d_2 c_2), \tag{3}$$

where ϵ_0 is the permittivity of a vacuum and D_w is the dielectric constant of water at the temperature of the experiment; the dielectric increments d_i are values similar to those quoted by Pethig (1979).

An electroosmotic mobility at the wall of $+12.5\times10^{-9}$ $m^2 \cdot V^{-1} \cdot s^{-1}$ was assumed. This value was determined by measuring the displacement of uncharged solutes in the same buffer and in a chamber exactly similar to the RAMSES chamber.

To compare the calculated results with the photometer measurements made during the observation phases of these experiments, the calculated protein distributions were converted into optical density values using coefficients that were measured during ground testing of the RAMSES equipment.

Figure 5 shows the photometer data for the different phases

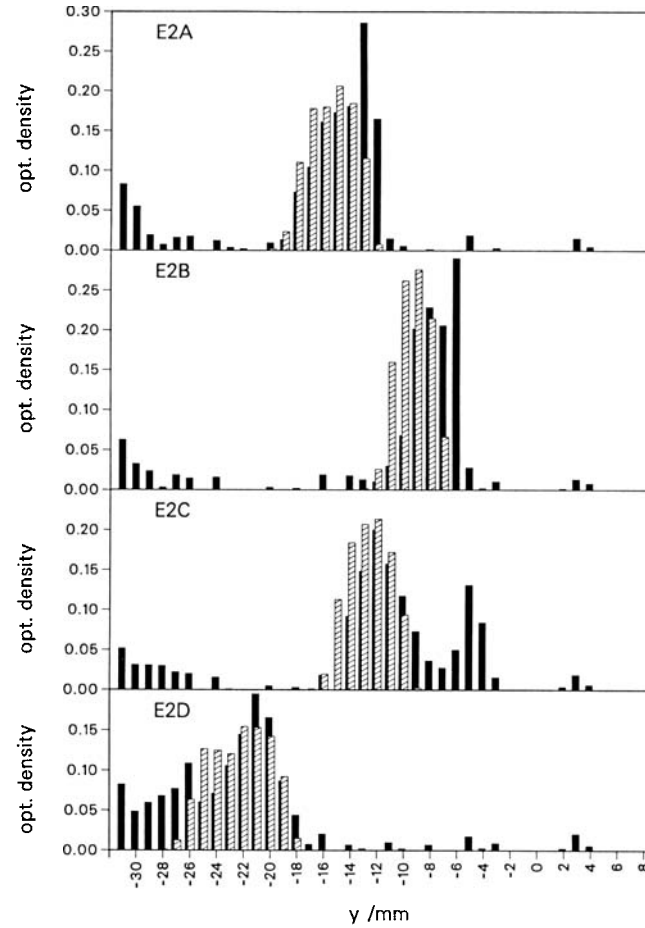

Figure 5. Optical densities: on-line UV photometer recording of the RAMSES facility during experiment E2 (■) vs. calculated results of the numerical model (▨).

The zero on the y axis gives the position of the protein under zero-field conditions, and the anode is on the left. The experimental conditions are given in Table 1.

of experiment E2. The optical density is shown as a function of the distance from the injection point, with the anode on the left of the figure. The experimental results are shown in black and the corresponding results of the model are shown as superimposed crosshatched bars. For these dilute solutions, the optical densities are relatively low and a certain amount of background noise is visible in the experimental measurements. The presence of small bubbles in the photometer cuvettes at the beginning of the operations prevented us from performing the in-flight calibration of the photometer that was scheduled: this may explain some of the noise and it is possible that the recorded signal is slightly distorted. However, the position of the protein filament does appear as a distinct peak in optical density. The optical density profiles were extremely stable during these microgravity experiments: they remained quite reproducible through several (4 to 6) photometer cycles, each cycle lasting almost 4 minutes. The rise in optical density on the left of each figure was consistently observed, both during the space experiments and during ground testing, whenever an electric field was applied; it is thought to be due to the accumulation of $(HOCH_2)_3CNH_3^+$ ions of the buffer at the membrane that closes off the anode compartment.

The agreement between the experimental and calculated results is quite satisfactory. In the phase E2C, a second peak appears in the experimental results that has not been accounted for. It was at first thought that it could be due to the protein filament breaking up under the influence of a strong electrohydrodynamic shear. However, the results of the numerical model indicate that under these conditions, the filament shows no signs of severe distortion.

The last phase of this experiment (E2D) was also that in which samples of the separated fractions were collected. The concentrations of protein in the fractions brought back were measured by gel phase liquid chromatography (GPLC), and the results of these measurements are shown in the lower part of Figure 6; the BSA concentrations are shown crosshatched and the α-lactalbumin concentrations are in black. In comparing these results with the photometer measurements in Figure 5, it should be remembered that UV light is more strongly absorbed by the α-lactalbumin than by the BSA. It can be seen that under the conditions applied in phase E2D, the two proteins are quite well separated: 83% of the α-lactalbumin, as well as 78% of the BSA, was recovered pure. The upper part of Figure 6 shows the protein distribution given in this case by the numerical model. The positions, widths, and relative heights of the two peaks are well predicted; the only point of difference is in the zone of overlap between the two peaks, which is more extensive in the calculated result. It can be seen in both cases that the α-lactalbumin peak has undergone more spreading than the BSA peak: it is wider and lower. The numerical model gives the explanation for this result: the contribution to the conductivity, for a similar concentration, is greater for the α-lactalbumin than for the BSA. Thus the BSA induces a weaker electrohydrodynamic effect and undergoes a lesser spreading. This difference is made clear in the present case because the two proteins were able to separate from each other at a sufficiently early stage in their progression through the chamber. Obviously two protein filaments that are close together undergo the electrodynamic movement taking place in the space

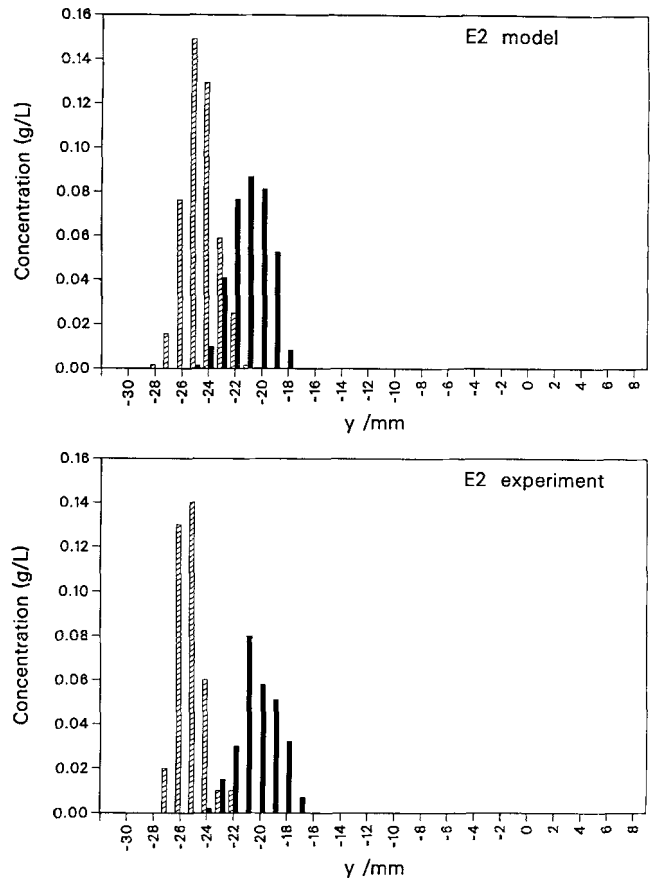

Figure 6. Protein concentrations in fractions: values collected during phase E2D of experiment E2 vs. by the numerical model.

The zero on the y axis gives the position of the protein under zero-field conditions, and the anode is on the left. The experimental conditions are given in Table 1.

where they are located. Whatever their contributions to the conductivity may be, if they are not sufficiently separated they will both be spread to the same degree. Even though the major part of the electrohydrodynamic spreading occurs early in the protein trajectory (when all filaments are necessarily close to each other), a separation that occurs at a sufficiently early stage can give rise to a difference in spreading between two proteins that have different conductivities.

The photometer measurements for experiment E3 are shown in Figure 7. As the initial sample solution for this experiment was ten times more concentrated than in experiment E2, it is not surprising to see that the optical densities in this experiment are much higher. However, as in experiment E2, they were found to be highly reproducible, though no comparison with earth-based tests is conceivable here as the sample is too concentrated to be used on earth. At this scale, the presence of noise is not so obtrusive and the accumulation of "tris" ions near the anode is less obvious. A small extraneous peak is still visible in the phase E3C at the same place as in E2C. Once again this observation has no clear explanation; even with this high-conductivity sample, the numerical model shows no tendency here for the filament to break up. The agreement between the experimental observations and the numerical calculations is once again quite satis-

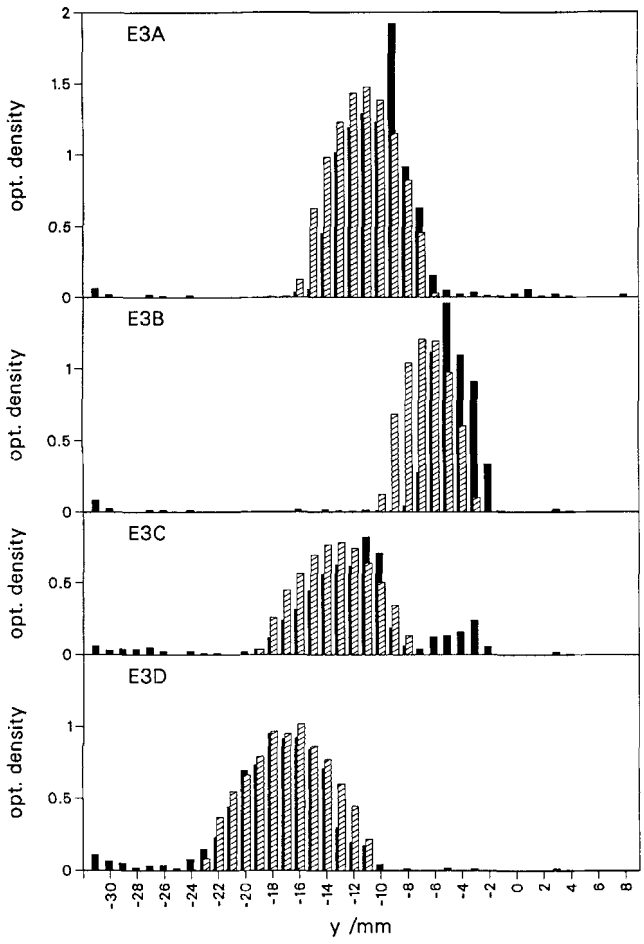

Figure 7. Optical densities: on-line UV photometer recording of the RAMSES facility during experiment E3 (■) vs. calculated results of the numerical model (▨).

The zero on the y axis gives the position of the protein under zero-field conditions, and the anode is on the left. The experimental conditions are given in Table 1.

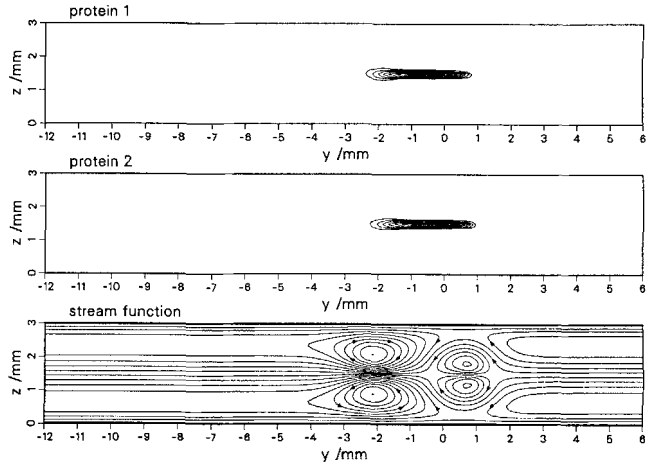

Figure 8. Concentration distribution for the two proteins and stream lines for the flow pattern of the numerical model for conditions of phase E3D for a plane situated 15 mm downstream from the injection point.

The chamber walls are represented by the upper and lower limits of each panel ($z = 0$ and $z = 3$ mm). The left and right boundaries (on the y axis) do not represent a physical barrier: they are arbitrarily fixed so as to be sufficiently far from the protein filament to prevent interference with the filament behavior.

factory, except in the phase E3B, where the model overestimates the extent of the migration. A comparison with the results of experiment E2 shows that the peaks are somewhat wider, but a tenfold increase in concentration has only caused a marginal increase in spreading. The numerical model shows that most of this spreading can be traced to the electrohydrodynamic effect, with a lesser contribution from molecular diffusion. The spreading due to the nonuniform residence times introduced by the Poiseuille flow and due to the electroosmotic flow (the "crescent" effect) is negligible in these experiments, as the filament diameter was kept small in comparison with the chamber thickness (about 20%).

Figure 8 shows the calculated distribution of the two proteins and the calculated flow pattern in a plane perpendicular to the carrier flow for the conditions in phase E3D. The chamber walls are situated at the top and bottom of each panel, while the limits to the right and left are open. This plane is located at only 15 mm from the injection point and the two proteins have migrated less than 1 mm, but the protein filament already shows the flattening and spreading that is typical of electrohydrodynamics. In the flow pattern, two contributions can be seen: the straight stream lines at either end of the calculation area show the electroosmotic flow with its parabolic profile. In the zone where the protein filament is located, there is a four-lobed recirculation pattern that is due to electrohydrodynamics. This pattern is particularly clear at this early stage in the separation: in fact, the electrohydrodynamic flow reaches its maximum in intensity within a few millimeters of the injection point and then subsides as the protein spreads and diffuses.

Fractions were collected once again during phase E3D. The protein concentrations in these fractions are shown in Figure 9. Only 26% of α-lactalbumin was recovered pure and all the BSA was at least slightly contaminated. The results of the numerical calculation are shown in the upper part of the figure. Once again the positions, widths, and relative heights of the two peaks are well predicted; about the same degree of overlap is found. One difference between the two results that may be significant is that the experimental distribution of α-lactalbumin has a double peak. A possible explanation for this can be found in the numerical results: the protein filament seems to have reached here the limit of its stability, under the effect of an intense electrohydrodynamic distortion. It is possible that in the experimental situation, where the environment is less ideal than in the calculation, the protein filament had begun to break up under the conditions applied here.

The numerical simulation shows that these more concentrated solutions could have been better separated by using a lower field strength together with a longer residence time. However, it is not certain that the trade-off of higher concentration treated against a lower production rate would be really advantageous. In any case, the experimental conditions used here were limited by the possibilities of the facility, and

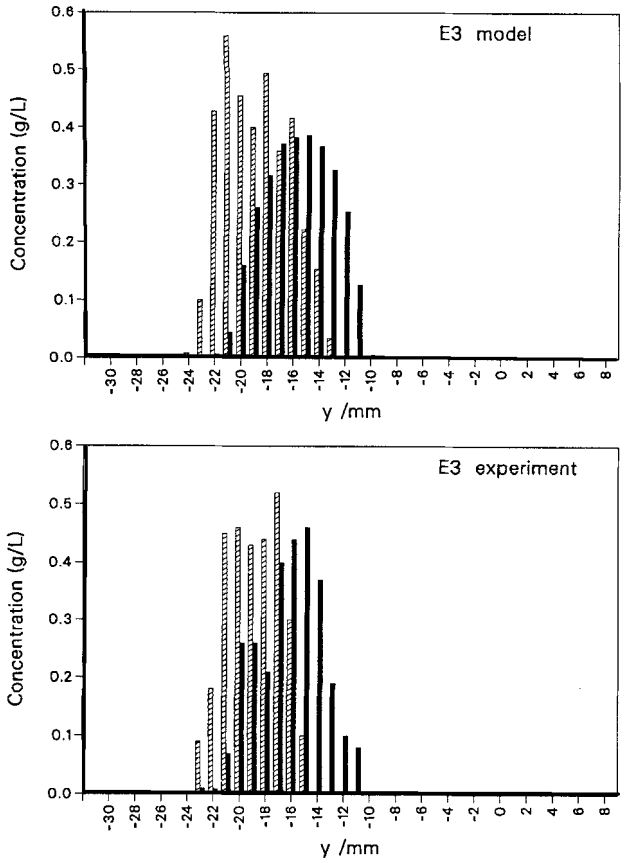

Figure 9. Protein concentrations in fractions: values collected during phase E3D of experiment E3 vs. by the numerical model.

The zero on the y axis gives the position of the protein under zero-field conditions, and the anode is on the left. The experimental conditions are given in Table 1.

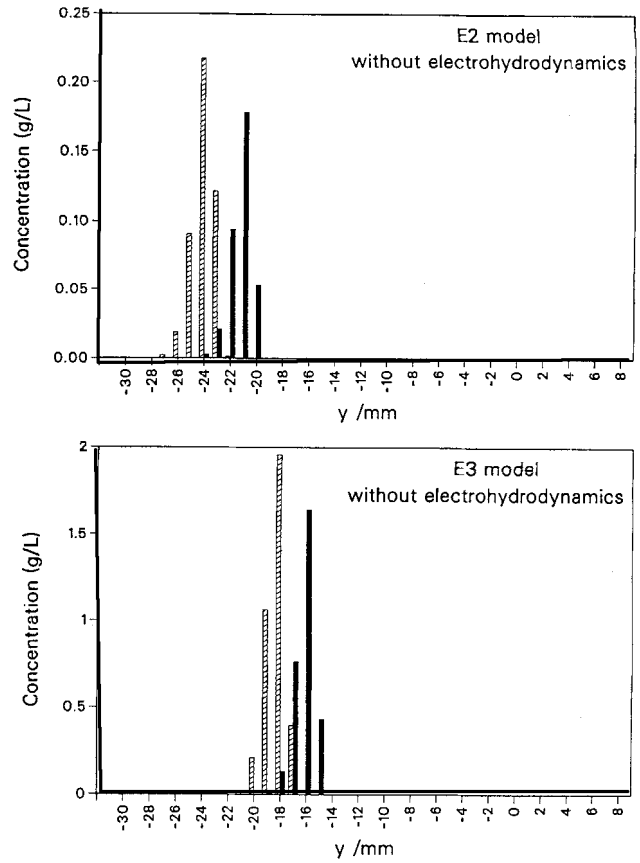

Figure 10. Numerical calculations performed with electrohydrodynamic movements suppressed: protein concentrations in the fractions collected for the phases E2D and E3D.

Compare these results with Figures 6 and 9, respectively.

it is not obvious that the creation of a very low, but perfectly regular, flow rate is a serious technological possibility.

The importance of the electrohydrodynamic effect can be judged from the concentration profiles given in Figure 10. These were calculated under the conditions for phases E2D and E3D using the same model, but with the electrohydrodynamic effect suppressed by setting all the λ_i, $[\eta]_i$, and d_i values to zero. They should be compared with the profiles in Figures 6 and 9, respectively. The difference is particularly striking for E3, where the concentrated sample was used: here each protein is spread over a small number of fractions, and so the final concentrations are much higher. In these two cases, the electrohydrodynamics has no clear effect on the protein displacement: the peaks are situated at roughly the same distance from the injection point as in Figures 6 and 9. A difference in the apparent migration distance has, however, been observed in simulations where one of the two solutes was assumed to make no contribution to conductivity.

Conclusion

The present experiments have shown the feasibility of performing electrophoretic separations in microgravity. This environment is particularly interesting as it allows the observation of electrophoretic separations without the interference of natural convection that disturbs this process on earth. A very satisfactory agreement was found between the experimental measurements and the numerical model, an agreement that is all the more remarkable as the model contains no adjustable parameters. This is the first time that such a detailed model of CFE has been applied to data obtained under such well-controlled conditions. The success of this project suggests that a fairly complete understanding of this process has now been attained. This should provide a basis for future optimization of the process. The fact that in protein separation, electrohydrodynamics plays such an important role in filament spreading should stimulate more research into ways of limiting this effect.

Acknowledgments

This work was financed by a grant from the CNES, the French Space Agency. The authors wish to thank the whole IML-2 crew for their help in making a success of RAMSES; they particularly wish to express their appreciation to the two mission specialists Leroy Chiao and Don Thomas for performing the RAMSES experiments with much intelligence and dedication.

Literature Cited

Clifton, M. J., "Numerical Simulation of Protein Separation by Continuous-flow Electrophoresis," *Electrophoresis*, **14**, 1284 (1993).

Clifton, M. J., and O. Marsal, "Heat Transfer Design of an Electrophoresis Experiment," *Acta Astronaut.*, **19**, 99 (1989).
Clifton, M. J., H. Roux-de Balmann, and V. Sanchez, "Electrohydrodynamic Deformation of the Sample Stream in Continuous-flow Electrophoresis with an AC Field," *Can. J. Chem. Eng.*, **70**, 1055 (1992).
Hannig, K., "Preparative Electrophoresis," *Electrophoresis: Theory, Methods and Applications*, Vol. II, M. Bier, ed., Academic Press, New York (1967).
Heinrich, J., M. J. Clifton, and H. Wagner, "Use of in situ Conductivity Measurements to Calculate the Flow Field and Heat Transfer in Continuous-Flow Electrophoresis," *Int. J. Heat Mass Transfer*, **36**, 3703 (1993).
Heinrich, J., and H. Wagner, "A Potential Gradient-Conductivity-Scanner for the Investigation of Effects Leading to Buoyancy-Driven Convection in Continuous-Flow Electrophoresis," *Adv. Space Res.*, **12**(1), 385 (1992).
Jouve, N., and M. J. Clifton, "Three-dimensional Modelling of the Coupled Flow Field and Heat Transfer in Continuous-flow Electrophoresis," *Int. J. Heat Mass Transfer*, **34**, 2461 (1991).
Pethig, R., *Dielectric and Electronic Properties of Biological Materials*, Wiley, Chichester, England (1979).
Rhodes, P. H., and R. S. Snyder, "Preparative Electrophoresis for Space," NASA Tech. Paper No. 2777, NASA, Washington, DC (1987).
Rhodes, P. H., R. S. Snyder, and G. O. Roberts, "Electrohydrodynamic Distortion of Sample Streams in Continuous-flow Electrophoresis," *J. Colloid Interface Sci.*, **129**, 78 (1989).
Smolarkiewicz, P. K., and W. W. Grabowski, "The Multidimensional Positive Definite Advection Transport Algorithm: Nonoscillatory Option," *J. Comput. Phys.*, **86**, 355 (1990).
Snyder, R. S., P. H. Rhodes, and T. Y. Miller, "Continuous-flow Electrophoresis System Experiments on Shuttle Flights STS-6 and STS-7," NASA Tech. Paper No. 2778, NASA, Washington, DC (1987).
Strickler, A., and T. Sacks, "Focusing in Continuous-flow Electrophoresis Systems by Electrical Control of Effective Cell Wall Zeta Potentials," *Ann. N.Y. Acad. Sci.*, **209**, 497 (1973).
Tyn, M. T., and T. W. Gusek, "Prediction of Diffusion Coefficients of Proteins," *Biotechnol. Bioeng.*, **35**, 327 (1990).

Appendix: Basis of the Numerical Model for Protein Separation by Elecrophoresis

The model will be presented here in the reduced form used in this work. For more detailed information see work by Clifton (1993).

At the steady state, a continuity condition applies for each protein solute:

$$\nabla \cdot \boldsymbol{J}_m = 0, \tag{A1}$$

where $\boldsymbol{J}_m$ is the flux of the species m. This parameter is expressed as the sum of three terms corresponding to the transport by migration, diffusion, and convection, respectively:

$$\boldsymbol{J}_m = -u_m c_m \nabla\phi - D_m \nabla c_m + \boldsymbol{V} c_m. \tag{A2}$$

Here u_m is the electrophoretic mobility of species m, c_m its concentration, D_m its diffusion coefficient, $\boldsymbol{V}$ the fluid velocity, and ϕ the electrical potential. The transport equation is parabolized by considering only the transport by convection in the direction of the carrier flow (x direction). It is then solved numerically using a flux-controlled-transport (FCT) algorithm (Smolarkiewicz and Grabowski, 1990) to avoid the effect of numerical diffusion.

The distribution of electrical potential is obtained by considering the charge-conservation condition, that is valid throughout the separation chamber:

$$\nabla \cdot \boldsymbol{j} = 0, \tag{A3}$$

where $\boldsymbol{j}$ is the current density vector. As the current is related to the potential gradient by the electrical conductivity of the solution κ, Eq. A3 can be written in the following form:

$$\nabla \cdot (\kappa \nabla\phi) = 0. \tag{A4}$$

This equation is solved by a finite-difference method in which the potential gradient in the direction of the carrier flow is neglected.

The electric field strength $\boldsymbol{E}$ is given by the potential gradient:

$$\boldsymbol{E} = -\nabla\phi. \tag{A5}$$

The flow velocity is calculated from the steady-state Navier–Stokes equation:

$$\nabla \cdot (\rho \boldsymbol{V}\boldsymbol{V} - \sigma) = 0, \tag{A6}$$

were σ is the stress tensor:

$$\sigma = -\left(p + \frac{\epsilon}{2}E^2\right)\boldsymbol{I} + \eta[\nabla \boldsymbol{V} + (\nabla \boldsymbol{V})^t] + \epsilon \boldsymbol{E}\boldsymbol{E}. \tag{A7}$$

Here p is the pressure, $\boldsymbol{E}$ the electric field vector, η the viscosity, and ϵ the dielectric permittivity of the medium. The superscript t indicates the transpose of a matrix. The last term in this equation is the electrohydrodynamic stress.

As the medium is incompressible, the following continuity condition applies to the velocity:

$$\nabla \cdot \boldsymbol{V} = 0. \tag{A8}$$

Eqs. A6, A7 and A8 were combined and expressed in terms of vorticity and stream function, taking into account the fact that both η and ϵ vary with the protein concentration (thus with position). The resulting equations can be linearized and parabolized by considering the nature of the flow: the momentum transfer in the x direction is dominated by convective transport, while in the other directions convective transport is negligible.

One of the boundary conditions is particularly important: there is a slip velocity at the wall due to electroosmotic move-

ment of the medium, that is, if d is the chamber half-thickness, at $z = 0$ and $z = 2d$,

$$V_y = -u_{os}\frac{\partial \phi}{\partial y}, \tag{A9}$$

where u_{os} is the electroosmotic mobility.

The electroosmotic flow is also involved in the definition of the boundary conditions for the flow at the two extremities of the y axis. At these two boundaries, the flow profile is the parabolic one imposed by the electroosmotic movement of the liquid:

$$V_y = u_{os}E_0\left[\frac{3}{2}\frac{z^2}{d^2} - 3\frac{z}{d} + 1\right], \tag{A10}$$

where E_0 is the strength of the electric field far from the disturbance created by the protein filament.

The final differential equations for the flow field were solved using a high-order finite-difference scheme. As all the equations have been parabolized in the direction of carrier flow, the calculation can be performed by a technique that advances from the inlet to the outlet plane.

Manuscript received June 28, 1995, and revision received Oct. 17, 1995.